ChemComm

COMMUNICATION

Plasmonic coupling of dual gold nanoprobes for SERS imaging of sialic acids on living cells†

Wanyao Song,‡ Lin Ding,‡ Yunlong Chen and Huangxian Ju*

Cite this: *Chem. Commun.*, 2016, 52, 10640

Received 17th May 2016,
Accepted 2nd August 2016

DOI: 10.1039/c6cc04147g

www.rsc.org/chemcomm

This work reports a benzoic group functionalized gold nanoflower as a bridge probe for both recognition of target sialic acids and assembly of poly(*N*-acetylneuraminic acid) modified gold nanoparticles, which leads to plasmonic coupling of two kinds of gold nanoprobes in a single-core–multi-satellite nanostructure to produce a sensitive surface-enhanced Raman scattering (SERS) signal for the imaging of sialic acids on living cells.

Glycans on cell surfaces include a vast variety of carbohydrate motifs attached to plasma membrane bound proteins or lipids,[1] and play crucial roles in many important physiological processes.[2] Among the common monosaccharide blocks that constitute glycan chains, sialic acids (SAs), a family of negatively charged 9-carbon monosaccharides, generally occupy the termini of these glycan chains,[3] and are widely expressed on higher eukaryote cell surfaces and take part in diverse biological processes.[4] The overexpression of SAs has been proven to correlate with several disease states such as cardiovascular diseases,[5] neurological diseases[6] and cancer.[7] Therefore, *in situ* visualization of global SAs on living cells is of great importance for the dynamic tracking of altered sialyltransferase expression closely associated with tumor malignancy, elucidation of the SA-regulated biological functions, and development of novel diagnostic and therapeutic approaches.

Great efforts have been made in the field of glycan imaging with fluorescence microscopy as the most popular technique. Recently, surface-enhanced Raman scattering (SERS) imaging has emerged as an alternative tool for glycan detection[8] because of its advantages of high sensitivity, non-destructive and non-invasive features, and fingerprinting capability on chemical structures.[9] Most of these strategies focus on either the design of 2D[8a] or 3D[8b] SERS substrates for positioning cells or the development of bioorthogonal Raman reporters.[8c] The sensitivity of these strategies is usually limited by the distance between the reporter and substrate or the absence of interparticle plasmonic coupling effects. To facilitate the improvement of the sensitivity, it is favorable to directly locate enormous Raman enhancement factors with short-range interactions on the target surface.[10]

These short-range interactions can be achieved *via* efficient interparticle plasmonic coupling, which has been considered as a significant contributor to the enhancement of Raman signals[11] by assembly of Au/Ag nanoparticles (NPs) with high density, including aggregation of AgNPs,[12a] binding of gold disks to a gold surface,[12b] formation of DNA–gold nanoaggregates,[12c] combination of polysaccharide-coated gold nanostars with Raman signal molecules and lectin dual-coded AuNPs,[12d] and recognition of aptamer-coated AuNPs and smaller Au nanoprobes for proteins and bound glycan.[12e] In this work, a novel Au nanoflower (AuNF) based probe was designed as a bridge to recognize target cell surface SAs and then assemble poly(*N*-acetylneuraminic acid) (PSA) and 5,5′-dithiobis(2-nitrobenzoic acid) (DTNB) modified poly(amidoamine) (PAMAM)-encapsulated AuNPs (DAuNPs), which form a single-core–multi-satellite nanostructure for the global imaging of SAs on living cells (Scheme 1). Both the coarse surface and dense tips of the AuNFs provided an increased surface area and large amounts of hot spots on their surfaces.[13] Thus the nanostructure produced strong SERS signals for sensitive imaging analysis of cell surface SAs.

The AuNFs were synthesized by quickly adding 1.0 mL $HAuCl_4$ solution (1%) into 50 mL sodium *N*-(2-hydroxyethyl)-piperazine-*N*′-(2-ethanesulfonate) (HEPES) (10 mM, pH 7.4) under continuous stirring at room temperature.[14] The TEM images showed a diameter of about 50 nm with good dispersibility and uniform size distribution of the AuNFs (Fig. 1A). Their UV-vis spectrum displayed a characteristic absorption peak at about 570 nm (Fig. 1B).

The AuNF based probe (3-MPBA/DTNB@AuNF) was obtained *via* co-functionalization of AuNF with DTNB as the Raman reporter and 3-MPBA as the SA recognition motif (ESI†). 3-MPBA can

State Key Laboratory of Analytical Chemistry for Life Science, School of Chemistry and Chemical Engineering, Nanjing University, Nanjing 210023, P. R. China. E-mail: hxju@nju.edu.cn

† Electronic supplementary information (ESI) available: Materials, methods, characterization and supplementary data. See DOI: 10.1039/c6cc04147g

‡ W. Y. Song and L. Ding contributed equally to this work.

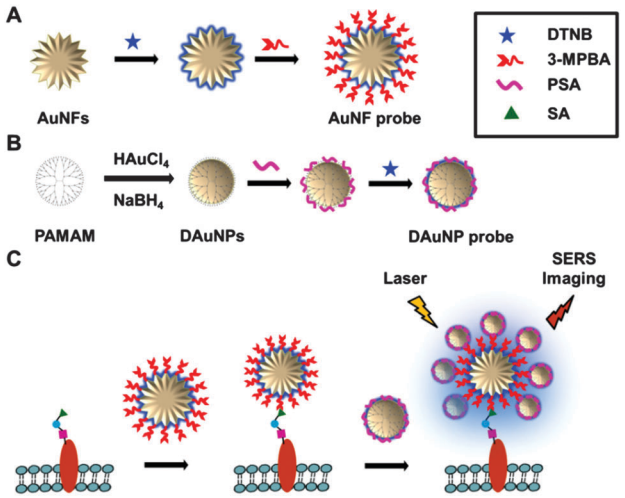

Scheme 1 Schematic illustration of (A) the preparation of the AuNF probe, (B) the preparation of the DAuNP probe, and (C) SERS imaging of the cell surface SAs based on plasmonic coupling of the core AuNF with the satellite AuNPs. 3-MPBA represents 3-mercaptophenylboronic acid.

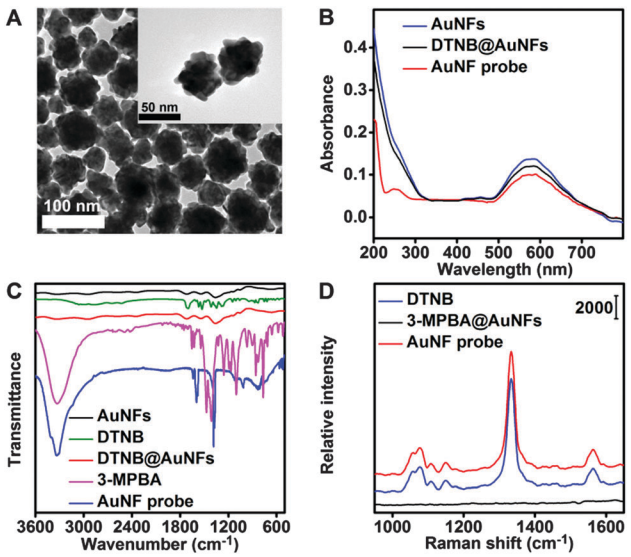

Fig. 1 (A) TEM images of the AuNFs. (B) UV-vis and (C) IR spectra of the AuNFs, DTNB, DTNB@AuNFs, 3-MPBA and AuNF probe. (D) Raman spectra of the solid powder of DTNB, 3-MPBA@AuNFs and the AuNF probe.

specifically bind C-8,9 diol of the SAs at the physiological pH of 7.4.[15] Thus the designed nanoprobe could act as a bridge to cell surface SAs and the PSA coated on AuNPs with much smaller size to form a single-core–multi-satellite nanostructure. Compared with lectin-based recognition of glycans on cell surfaces, the chemoselective recognition of the benzoic group to SA possesses higher affinity and is independent of metabolism of the biological system, thus it can be used for comparing SA expression levels among different cell lines.

The step-by-step assembly of the AuNF probe was demonstrated with infrared (IR) spectra (Fig. 1C). The AuNF probe showed characteristic bands for 3-MPBA, such as the hydroxyl group around 3334 cm^{-1}, benzene ring around 1604 cm^{-1} and carbon–boron bond around 1382 cm^{-1} (blue curve).[16] The weak peak at 2554 cm^{-1} for the thiol of 3-MPBA (purple curve) disappeared, while a 16 cm^{-1} red shift of the benzene ring peak and a 20 cm^{-1} red shift of the carbon–boron bond of 3-MPBA were observed upon binding to AuNF (blue curve), which might be attributed to the effect of the formed Au–S bond on these bonds. The IR signals of DTNB from the carbonyl group (1701 cm^{-1}) and nitroso group (1553 and 1362 cm^{-1}) were very weak (green curve), and were covered by the absorption of both AuNFs (red curve) and 3-MPBA (blue curve). However, the Raman spectrum of the AuNF probe (red curve in Fig. 1D) showed three peaks of DTNB at 1079, 1330 and 1569 cm^{-1}, which were consistent with DTNB powder (blue curve in Fig. 1D), demonstrating the conjugation of DTNB on AuNFs.

For satellite probe preparation, the size of the AuNPs was controlled using a generation 5.0 PAMAM dendrimer (G5-NH_2) with a molecular size of 5.7 nm as both the template and the stabilizer for the AuNP synthesis.[17] The formation of intradendrimer complexes between the dendrimer and Au ions facilitated the formation of size-monodisperse dendrimer-encapsulated AuNPs (DAuNPs) at room temperature. These DAuNPs were co-modified with DTNB and poly(*N*-acetylneuraminic acid) (PSA) to produce DAuNP probes, which could specifically bind to the AuNF probe *via* the interaction of PSA and the benzoic groups on the AuNF surface.

To achieve efficient SERS enhancement by the designed single-core–multi-satellite nanostructure, the control of both size and monodispersity of the satellite DAuNPs was important. The dendrimer with uniform composition and structure offered a desirable template to confine and stabilize the intradendrimer nanoparticle.[18] Moreover, the surface of the encapsulated nanoparticles was unpassivated and accessible for further modification *via* the Au–S bond.[19] The successful synthesis of DAuNPs in the presence of PAMAM G5-NH_2 was verified using a TEM image (inset in Fig. 2A) and UV-vis spectrum (Fig. 2A). The DAuNPs exhibited a globular-shape with a monodisperse size of about 3 nm. The distinctive plasmon band for the AuNPs disappeared in the adsorption spectrum of the DAuNPs (Fig. 2A), which is a common phenomenon for AuNPs with small diameter.[20] In the absence of dendrimer during the synthesis, the plasmonic band was obvious for the prepared AuNPs, suggesting that a larger

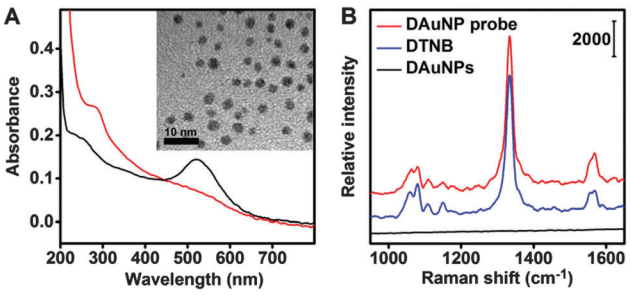

Fig. 2 (A) UV-vis spectra of the AuNPs prepared by reduction of chloroauric acid by $NaBH_4$ in the presence (red) and absence (black) of the dendrimer. Inset in (A): TEM image of DAuNPs. (B) Raman spectra of the solid powder of DTNB, DAuNPs and the DAuNP probe.

nanoparticle was obtained without confinement by the dendrimer. After the modification of the DAuNPs, the obtained DAuNP probe showed a similar Raman spectrum outline to pure DTNB (Fig. 2B), indicating that DTNB was assembled on the DAuNPs.

The assembly of the DAuNP probe on the AuNF probe was demonstrated by comparing the TEM images of the AuNF probe before (inset in Fig. 1A) and after (inset in Fig. S1, ESI†) treatment with the DAuNP probe. The latter showed multiple DAuNP satellites around the core AuNF probe. In order to verify the feasibility of the proposed strategy, a series of control experiments were performed (Fig. S1A, ESI†). AuNPs with a diameter of 40 nm were prepared and used to replace the AuNFs for fabricating the control AuNP probe. AuNFs did not exhibit any Raman response (line a), because of the absence of a Raman reporter.

Compared with the AuNP probe (curve b), the AuNF probe showed a higher intensity at the characteristic peaks of DTNB (curve c), suggesting a stronger SERS effect with AuNFs. This result could be attributed to more hot spots existing on AuNFs for a localized near-field enhancement effect.[10] The plasmonic coupling effect was further demonstrated by adding the DAuNP probe to the AuNF probe to form the single-core–multi-satellite nanostructure, which displayed a tremendously enhanced signal (curve f) compared with the AuNF probe alone (curve c), indicating the occurrence of strong plasmonic coupling of the enormous hot spots. The AuNF probe without DTNB (curve d) or the DAuNP probe without DTNB (curve e) was also employed to mix with the DAuNP probe and the AuNF probe, respectively. Both mixtures showed lower signals compared with curve f, due to less Raman reporter loaded in the nanostructure. However, the influence of the DTNB amount was less significant compared with that from the plasmonic coupling. The satellite binding-based enhancement could be theoretically demonstrated using electromagnetic simulation with a finite-difference time domain (FDTD) method[11] (Fig. S2, ESI†). The enhancement in the gap (5 nm) between the core AuNF and satellite AuNP suggested the occurrence of strong plasmonic coupling.

The amount of PSA and DTNB for the preparation of the DAuNP probe was optimized to be 100 μL of 1% PSA in 10 mL of DAuNP solution (2.0 μM) and 10 pmol DTNB in 1 mL of PSA@DAuNP solution (20 nM) (Fig. S3, ESI†). The amount ratio of the DAuNP probe to the AuNF probe added to form the single-core–multi-satellite nanostructure was optimized to be 50 : 1, at which the greatest enhancement was obtained (Fig. S1B, ESI†). This result also indicated that more DAuNP probe wrapped on the AuNF probe could contribute to a higher SERS signal due to a stronger plasmonic coupling and more Raman reporter involved in the nanostructure.

The feasibility of using the single-core–multi-satellite nanostructure for SERS imaging of cell surface SA was investigated. The AuNF probe could specifically bind to cell surface SAs using the chemoselective covalent linkage between the benzoic groups on the AuNF probe and the diol structure of the SAs. The intensity of the SERS signal increased obviously with the extended incubation time of the AuNF probe with cells (Fig. S1C and Fig. S4, ESI†), and 60 min was selected. After adding the DAuNP probe to the AuNF probe-bound cells, the DAuNP probe could be captured by the AuNF probe, which led to an obviously elevated Raman intensity (Fig. S1D and Fig. S5, ESI†) due to the generation of plasmonic coupling of hot spots. Owing to the blocking effect of cells, only a part of the surface of the AuNF probe was accessible for the DAuNP probe, which resulted in weaker enhancement than that obtained in solution (Fig. S1A, ESI†). The reaction time of the DAuNP probe was chosen as 60 min, at which the intensity of the SERS signal reached a plateau (Fig. S1D, ESI†). The cells exhibited a viability of ~98% after sequential binding by the AuNF and DAuNP probes (Fig. S6, ESI†), suggesting an excellent cytocompatibility of these probes.

The high sensitivity of the proposed SERS imaging strategy for the cell surface SAs enabled dynamic monitoring of the variation of SA expression on living cells in response to drug treatment. Sialidase was chosen as the model drug that can cleave the SAs on the cell surface. The MCF-7 cells were firstly treated with sialidase over different times, and then incubated with the two probes successively. Compared with untreated MCF-7 cells, the SERS intensity of the sialidase-treated cells decreased obviously with longer treatment times (Fig. 3), and reached only 4.5% of untreated cells after a 30 min cleaving time. This result also demonstrated the specificity of the proposed strategy. For a cell surface without SA expression, only a tiny signal was obtained, indicating that the observed signal before drug treatment was entirely from the nanostructure specifically bound to the cell surface SAs.

The recognition specificity was further validated by *N*-acetylneuraminic acid (Neu5Ac) inhibition testing (Fig. S7, ESI†). The AuNF probe was pretreated by reaction with excessive Neu5Ac for 1 h, thus the recognition sites on the AuNF probe were blocked. After incubating MCF-7 cells with the Neu5Ac-pretreated AuNF probe followed by the DAuNP probe, the Raman intensity of the cells almost disappeared, suggesting a specific recognition between the AuNF probe and the SAs on the cell surface.

To further demonstrate the contribution of more hot spots by the AuNFs for SERS imaging of cell surface SAs, a control AuNP probe was used to incubate the cells. As shown in Fig. S8 (ESI†), after incubation with the DAuNP probe or the AuNP probe alone, the cells exhibited tiny and weak Raman signals, respectively.

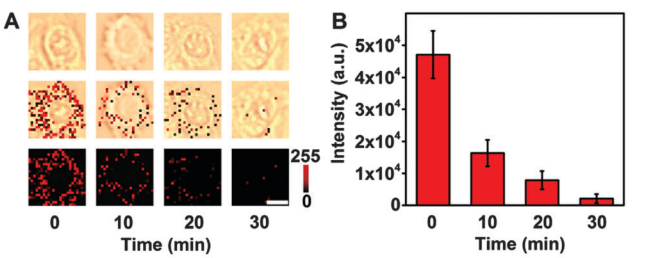

Fig. 3 (A) Bright field, overlay and Raman images and (B) the corresponding Raman intensities of MCF-7 cells pretreated with 25 mU mL^{-1} sialidase at 37 °C for different times followed by incubation with the two probes. Scale bar: 10 μm.

The signal obtained from the AuNP probe was only 48.2% of that from the AuNF probe, suggesting more hot spots on the AuNF probe compared with the AuNP probe. After subsequent incubation of AuNP probe-bound cells with the DAuNP probe, the Raman intensity increased, and the obtained signal was 43.3% of that when the AuNF–DAuNP nanostructure was used. These results suggested the excellent SERS sensitivity of the designed single-core–multi-satellite nanostructure for Raman imaging.

The feasibility of the proposed strategy for other cell lines was further demonstrated using normal HaCaT cells as a model. After successive incubation with the two probes, HaCaT cells exhibited much weaker signals under the same conditions compared with MCF-7 cells (Fig. 4), which indicated that the SAs on the surface of the MCF-7 cells were highly over-expressed compared to those on the surface of the HaCaT cells. The results were consistent with previous reports,[21] and suggested that the strategy was suitable for various cell types and could be used for distinguishing cancer cells from normal cells.

In summary, this study describes the development of a novel single-core–multi-satellite nanostructure for sensitized SERS imaging of cell surface SAs using a designed benzoic group functionalized gold nanoflower as a bridge probe. With the bridge-type binding, this nanostructure can be introduced to cell surface SAs by specific chemoselective recognition, thus contributing to the sensitive and specific mapping of SAs on living cells. This nanostructure possesses enormous "hot spots" to produce a strong plasmonic coupling effect for the enhancement of the SERS signal. The proposed strategy has been employed to monitor the dynamic change in SA levels on cell surfaces and is suitable for other cell lines. This method could be conveniently adapted to other glycan motifs through the integration of the single-core–multi-satellite nanostructure with other glycan labeling techniques.

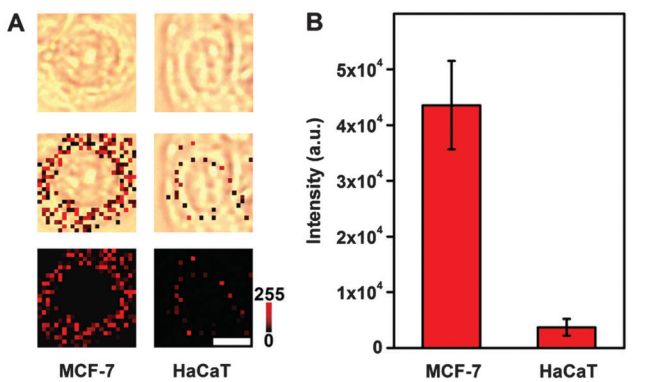

Fig. 4 (A) Bright field, overlay and Raman images and (B) the corresponding Raman intensities of MCF-7 and HaCaT cells after incubation with the two probes. Scale bar: 10 μm.

We gratefully acknowledge the National Natural Science Foundation of China (21135002, 21322506) and the National Basic Research Program (2014CB744501).

Notes and references

1 K. Ohtsubo and J. D. Marth, *Cell*, 2006, **126**, 855–867.
2 J. D. Marth and P. K. Grewal, *Nat. Rev. Immunol.*, 2008, **8**, 874–887.
3 (*a*) A. L. Lewis, N. Desa, E. E. Hansen, Y. A. Knirel, J. I. Gordon, P. Gagneux, V. Nizet and A. Varki, *Proc. Natl. Acad. Sci. U. S. A.*, 2009, **106**, 13552–13557; (*b*) A. Matsumoto, H. Cabral, N. Sato, K. Kataoka and Y. Miyahara, *Angew. Chem., Int. Ed.*, 2010, **49**, 5494–5497.
4 X. Chen and A. Varki, *ACS Chem. Biol.*, 2010, **5**, 163–176.
5 G. Lindberg, G. A. Eklund, B. Gullberg and L. Rastam, *BMJ*, 1991, **302**, 143–146.
6 A. Varki, *Trends Mol. Med.*, 2008, **14**, 351–360.
7 (*a*) S. Hakomori, *Cancer Res.*, 1996, **56**, 5309–5318; (*b*) D. H. Dube and C. R. Bertozzi, *Nat. Rev. Drug Discovery*, 2005, **4**, 477–488; (*c*) Y. F. Xu, A. Sette, J. Sidney, S. J. Gendler and A. Franco, *Immunol. Cell Biol.*, 2005, **83**, 440–448.
8 (*a*) M. Tabatabaei, G. Q. Wallace, F. A. Caetano, E. R. Gillies, S. S. G. Ferguson and F. Lagugne-Labarthet, *Chem. Sci.*, 2016, **7**, 575–582; (*b*) T. Gong, Y. Cui, D. Goh, K. K. Voon, P. P. Shum, G. Humbert, J. L. Auguste, X. Q. Dinh, K. T. Yong and M. Olivo, *Biosens. Bioelectron.*, 2015, **64**, 227–233; (*c*) M. Xiao, L. Lin, Z. Li, J. Liu, S. Hong, Y. Li, M. Zheng, X. Duan and X. Chen, *Chem. – Asian J.*, 2014, **9**, 2040–2044.
9 (*a*) Y. Wang, B. Yan and L. Chen, *Chem. Rev.*, 2013, **113**, 1391–1428; (*b*) D. Graham and R. Goodacre, *Chem. Soc. Rev.*, 2008, **37**, 883–884; (*c*) M. Y. Sha, H. Xu, M. J. Natan and R. Cromer, *J. Am. Chem. Soc.*, 2008, **130**, 17214–17215.
10 X. Qian, X. Zhou and S. Nie, *J. Am. Chem. Soc.*, 2008, **130**, 14934–14935.
11 Y. Zhu, X. Jiang, H. Wang, S. Wang, H. Wang, B. Sun, Y. Su and Y. He, *Anal. Chem.*, 2015, **87**, 6631–6638.
12 (*a*) J. J. Liang, H. W. Liu, C. H. Huang, C. Z. Yao, Q. Q. Fu, X. Q. Li, D. L. Cao, Z. Luo and Y. Tang, *Anal. Chem.*, 2015, **87**, 5790–5796; (*b*) L. Feuz, M. P. Jonsson and F. Hook, *Nano Lett.*, 2012, **12**, 873–879; (*c*) Y. Li, X. D. Qi, C. C. Lei, Q. F. Yue and S. S. Zhang, *Chem. Commun.*, 2014, **50**, 9907–9909; (*d*) Y. L. Chen, L. Ding, J. Q. Xu, W. Y. Song, M. Yang, J. J. Hu and H. X. Ju, *Chem. Sci.*, 2015, **6**, 3769–3774; (*e*) Y. L. Chen, L. Ding, W. Y. Song, M. Yang and H. X. Ju, *Chem. Sci.*, 2016, **7**, 569–574.
13 Q. Li, Y. Jiang, R. Han, X. Zhong, S. Liu, Z. Y. Li, Y. Sha and D. Xu, *Small*, 2013, **9**, 927–932.
14 J. Xie, Q. Zhang, J. Y. Lee and D. I. C. Wang, *ACS Nano*, 2008, **2**, 2473–2480.
15 (*a*) A. Matsumoto, H. Cabral, N. Sato, K. Kataoka and Y. Miyahara, *Angew. Chem., Int. Ed.*, 2010, **49**, 5494–5497; (*b*) H. Otsuka, E. Uchimura, H. Koshino, T. Okano and K. Kataoka, *J. Am. Chem. Soc.*, 2003, **125**, 3493–3502; (*c*) A. Matsumoto, N. Sato, K. Kataoka and Y. Miyahara, *J. Am. Chem. Soc.*, 2009, **131**, 12022–12023.
16 M. Eguilaz, R. Villalonga, J. M. Pingarron, N. F. Ferreyra and G. A. Rivas, *Sens. Actuators, B*, 2015, **216**, 629–637.
17 (*a*) R. M. Crooks, M. Q. Zhao, L. Sun, V. Chechik and L. K. Yeung, *Acc. Chem. Res.*, 2001, **34**, 181–190; (*b*) A. R. Menjoge, R. M. Kannan and D. A. Tomalia, *Drug Discovery Today*, 2010, **15**, 171–185.
18 J. C. Garcia-Martinez and R. M. Crooks, *J. Am. Chem. Soc.*, 2004, **126**, 16170–16178.
19 X. Wang, X. Cai, J. Hu, N. Shao, F. Wang, Q. Zhang, J. Xiao and Y. Cheng, *J. Am. Chem. Soc.*, 2013, **135**, 9805–9810.
20 Y. G. Kim, S. K. Oh and R. M. Crooks, *Chem. Mater.*, 2004, **16**, 167–172.
21 X. Zhang, B. Chen, M. He, Y. Zhang, L. Peng and B. Hu, *Analyst*, 2016, **141**, 1286–1293.